Synthesis of a Pd on Ni–B nanoparticle catalyst by the replacement reaction method for hydrodechlorination

Zhijie Wu, Minghui Zhang *, Zongfang Zhao, Wei Li, Keyi Tao

Institute of New Catalytic Materials Science, College of Chemistry and Engineering Research Center of High-Energy Storage and Conversion (Ministry of Education), Nankai University, Tianjin 300071, PR China

ARTICLE INFO

ABSTRACT

A Pd on Ni–B (Pd/Ni–B) bimetallic nanoparticle catalyst was prepared through a replacement reaction of amorphous Ni–B nanoparticles with Pd^{2+} ions. In the hydrodechlorination of chlorobenzene, the Pd/Ni–B bimetallic catalyst exhibited better activity than a Pd catalyst supported on polyvinylpolypyrrolidone, a mixture of Pd and Ni–B nanoparticles, and a Pd on Ni catalyst obtained by the replacement reaction of nanocrystalline Ni with Pd^{2+} ions. The properties of the Pd/Ni–B catalyst were studied in detail by XRD, TEM, XPS, and H_2 chemisorptions. The characterizations demonstrated that a Pd–Ni–B surface alloy occurred on the Pd/Ni–B catalyst with heating treatment. The resulting surface alloy promoted resistance to chlorine poisoning, adsorption of the reactants (chlorobenzene and hydrogen), and desorption of products, explaining the better catalytic activity and stability of the Pd/Ni–B bimetallic catalyst.

© 2008 Elsevier Inc. All rights reserved.

1. Introduction

The dehalogenation of the carcinogenic and mutagenic aromatic halides has attracted much attention [1–3]. Aromatic chlorides are much less reactive than aromatic bromides and iodides [4], and few effective methods are available for the dechlorination (DC) of aromatic chlorides [5]. The most attractive and efficient DC method is catalytic hydrodechlorination (HDC), in which a variety of catalysts (e.g., Rh, Pt, Pd, Ni, Cu) and gaseous hydrogen or alcohols (as hydrogen donor) are used [6]. HDC is emerging as a nondestructive alternate technology in which chlorinated waste can be converted into products of commercial value [1,7]. Among the HDC catalysts, Pd-based catalysts have been widely investigated because of their superior catalytic properties [8,9].

Bimetallic nanoparticle catalysts have received increasing attention over the last 50 years. The addition of the second metal plays a key role in controlling the activity, selectivity, and stability of catalysts in certain reactions [10]. Recently, a Pd on Au bimetallic nanoparticle catalyst for the HDC of trichloroethene was prepared by adding controlled amounts of Pd salt and a reducing agent to an Au sol [11,12]. The resulting catalyst demonstrated excellent catalytic properties by distributing Pd atoms homogeneously over the Au surface and producing a synergistic effect of Pd with Au. The Pd on Au bimetallic catalyst structure provides a new synthesis approach in improving the catalytic properties of monometallic Pd materials [11]. Other than the chemical reduction, the replacement

reaction also is used to prepare bimetallic nanoparticles [13–17], and some bimetallic nanoparticles have shown improved catalytic properties [18–21]. The replacement reaction is defined as a reaction of a metal ion with a more reactive metal solid. Amorphous Ni–B nanoparticle is characteristic of a unique short-range ordering structure but a long-range disordering structure, along with a high concentration of coordinatively unsaturated sites. It demonstrates better catalytic activity and selectivity than its corresponding crystalline counterparts [22,23]. In the present work, a Pd on Ni–B (Pd/Ni–B) bimetallic nanoparticle catalyst was synthesized by reacting solutions of $Na_2[PdCl_4]$ with amorphous Ni–B nanoparticle instead of nanocrystalline Ni. Its catalytic performance in the HDC of chlorobenzene was examined and compared with that of Pd supported on polyvinylpolypyrrolidone (PVP) and Pd on Ni (Pd/Ni) bimetallic nanoparticles from the replacement of crystalline Ni nanoparticles by Pd. The correlation with the structural characteristics was investigated.

2. Experiments and methods

2.1. Catalyst preparations

Amorphous Ni–B nanoparticles were prepared by a modified chemical reaction. In a typical synthesis, 11.1 ml of ethylenediamine was dissolved in 1800.0 ml of deionized water, and then 21.8 g of $NiCl_2 \cdot 6H_2O$ and 9.0 g of KBH_4 were added to the ethylenediamine aqueous solution under stirring. The pH of the solution was controlled at 12.5–13.0 by the addition of NaOH. To prepare amorphous Ni–B nanoparticles, the solution was heated to

---

* Corresponding author. Fax: +86 22 2350 7730.
E-mail address: zhangmh@nankai.edu.cn (M. Zhang).

$70 \pm 1.0\,^\circ$C. The reaction lasted until no bubbles were observed, and the resulting black solid was washed free of inorganic ions and organic substances with deionized water and ethanol. Crystalline Ni nanoparticles were prepared by the reduction of Ni^{2+} by hydrazine as described previously to [24]. First, 1.0 g of $NiCl_2 \cdot 6H_2O$ (0.0042 mol) was dissolved in 7.5 ml of ethanol in a beaker; then 4.0 g of 50% $N_2H_4 \cdot H_2O$ (0.04 mol) was mixed with 2.5 g of NaOH by stirring, and the resulting slurry was added to the beaker. The reaction was initiated by adding a small amount of inducing agent, KBH_4, which reduced Ni^{2+} to metal nanoparticles that catalyzed the reaction between Ni^{2+} and hydrazine at 25 °C. The black precipitate was washed with ammonia, deionized water, and finally acetone.

A PVP-supported Pd catalyst was synthesized as described previously [25,26]. To a solution of 0.055 g of $PdCl_2$ in 1.0 ml of 5 mol/L NaCl, 50.0 ml of absolute ethanol and 0.7 g of PVP were added. The resulting red-brown solution of $PVP-PdCl_2$ (6.3×10^{-3} µmol/L Pd, N/Pd = 20 [molar ratio]) was stirred for 48 h at room temperature and then reduced by a 1 mol/L KBH_4 solution under a 40-ml/min N_2 flow. The product was washed with water and ethanol and then collected by centrifugation. For the preparation of Pd/Ni–B or Pd/Ni bimetallic catalysts, 0.055 g of $PdCl_2$ was dissolved in 50.0 ml of 0.1 mol/L NaCl solution under the N_2 atmosphere, after which the Ni–B or crystalline Ni was added to the $Na_2[PdCl_4]$ solution and stirred for 4 h. The Pd loading was selected at a weight ratio of 1/99 (Pd/Ni).

The supported catalysts were prepared as follows. The Ni–B/TiO_2 was prepared as described previously [27,28]. Then 0.02 g of silver nitrate, 0.15 g of ammonium hydroxide, 0.005 g of sodium hydroxide, and 0.002 g of formaldehyde were dissolved in 425.0 ml of distilled water, after which 6.39 g of titania (anatase, 27 m²/g) was added to this solution. After stirring at 40 °C for 4 h, the resulting Ag/TiO_2 was washed with distilled water and dried at 80 °C for 4 h. The electroless Ni–B plating solution comprised nickelous sulfate hexahydrate (12 g/L), ethylenediamine (12 g/L), and potassium borohydride (5.5 g/L). The pH value of the solution was adjusted to 13.5 by NaOH. To prepare the supported Ni–B/TiO_2 catalyst, 2.0 g of Ag/TiO_2 was added to 150.0 ml of as-prepared Ni–B plating solution under stirring at 50 °C. The reaction lasted until no significant bubbles were observed. The resulting samples were washed thoroughly with distilled water until a pH of 7 was achieved, then washed with absolute alcohol. For the preparation of supported Pd/Ni–B/TiO_2 catalyst, 0.055 g of $PdCl_2$ was dissolved in 50.0 ml of 0.1 mol/L NaCl solution under the N_2 atmosphere. Then the Ni–B/TiO_2 was added to the $Na_2[PdCl_4]$ solution, stirred for 4 h, and washed as described above. The ICP results revealed the following weight ratio of the components in the Pd/Ni–B/TiO_2: 0.1% Pd: 1.5% B: 10.4% Ni: 87.5% TiO_2.

2.2. Reaction

The HDC of chlorobenzene was carried out in a 100-ml autoclave in which the catalysts containing 0.1 mmol Pd, 50.0 mmol of chlorobenzene, 0.5 g NaOH, and 50.0 ml of ethanol were mixed. Before the HDC reaction, the catalysts were treated with a 40-ml/min N_2 flow at 25, 200, 300, and 400 °C for 2 h. The HDC reaction was carried out at 90 °C. The hydrogen pressure in all experiments was 1.0 MPa. The products were analyzed with a gas chromatograph equipped with a flame ionization detector. The results demonstrated formation of only benzene and HCl; thus, either benzene yield or chlorobenzene conversion was used to evaluate the HDC activity.

HDC was performed without the use of catalyst (blank experiment), and ethanol's HDC/DC capability was evaluated by carrying out the HDC reaction without hydrogen or catalyst. Both the conversion of chlorobenzene without the use of catalyst and the
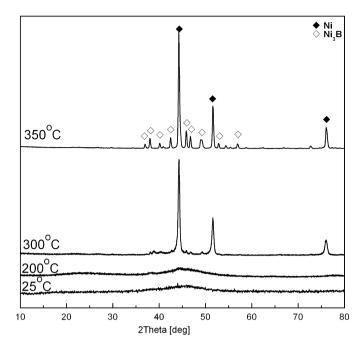

Fig. 1. XRD patterns of Pd/Ni–B catalysts treated in a 40-ml/min N_2 flow at different temperatures for 1 h.

HDC/DC capability of ethanol were <0.1%, suggesting that ethanol served as a solvent and did not promote HDC activity of the catalyst.

2.3. Characterization

Powder X-ray diffraction (XRD) patterns of the catalysts were obtained on a Rigaku D/max 2500 X-ray diffractometer (Cu $K\alpha$, $\lambda = 1.54178$ Å). The compositions of the samples were measured by inductively coupled plasma atomic emission spectrometry (ICP-AES) on an IRIS Intrepid spectrometer. Transmission electron microscope (TEM) images were obtained with an FEI Tecnai G2 high-resolution transmission electron microscope. X-ray photoelectron spectroscopy (XPS) analysis of the catalysts was carried out using a Kratos Axis Ultra DLD spectrometer using a monochromatic Al $K\alpha$ source, hybrid magnetic/electrostatic optics, and a multichannel plate and delay line detector (DLD). The surface of the samples was etched with Ar^+ ions for 15 min to remove the oxidated layer. Temperature-programmed desorption (TPD) of hydrogen, benzene, or chlorobenzene was performed as follows: The surface of the sample (20 mg) was purged by a flow of ultra-pure argon (99.999%) for 2 h at 200 °C. (The temperature was kept relatively low to avoid crystallization of the amorphous catalysts.) Once the catalyst was cooled to 25 °C in argon, H_2, chlorobenzene, or benzene was introduced to the catalyst for adsorption. After 12 h, desorption of the adsorbate was performed under an argon flow of 30 ml/min. All gases were of ultra-high purity and were further purified by a Chrompack clean-oxygen filter and molecular sieve. The temperature was raised from 25 to 600 °C at a rate of 10 °C/min.

3. Results

3.1. Characterization

The atom composition of amorphous Ni–B nanoparticle was $Ni_{67.4}B_{32.6}$, and the Pd loading on Pd/Ni–B catalyst was 0.8 wt%. It was well known that many metal oxides or salts can be spontaneously dispersed on the surface of oxide supports to form
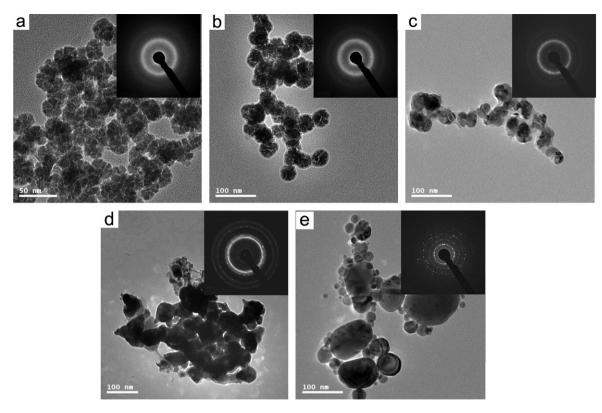
Fig. 2. TEM images of (a) Ni–B, (b) Pd/Ni–B treated at 25 °C, (c) Pd/Ni–B treated at 200 °C, (d) Pd/Ni–B treated at 300 °C, and (e) Pd/Ni–B treated at 350 °C in a flow of 40 ml/min N_2.

a monolayer due to the formation of interfacial chemical bonds [18–20]. Wang et al. found that a metal can disperse on the surface of another metal to form a highly dispersed bimetallic system due to the formation of bonds between the two metals. They noted that a highly dispersed Pd–Ni system occurred when <2.0 wt% Pd was loaded on a Pd/Ni catalyst [19]. In the present work, XRD was used to characterize the structure of the Pd/Ni–B bimetallic nanoparticles. No diffraction peak corresponding to crystalline Pd was found, indicating a high dispersion of Pd. Figs. 1a and 1b show a broad, featureless peak at around $2\theta = 45°$ indicating the amorphous structure of Pd/Ni–B bimetallic nanoparticles treated at 25 and 200 °C. Increasing the treatment temperature to 300 °C led to the appearance of peaks corresponding to crystalline Ni; on a further increase to 350 °C, the Ni_3B phase appeared. Peaks due to crystalline Pd or to Pd compounds still were not seen, however.

Fig. 2 presents a series of TEM micrographs of samples heated at different temperatures. Fig. 2a shows spherical, flower-shaped Ni–B particles of ∼30 nm. The SAED pattern (insert in Fig. 2a) indicates the amorphous nature of these particles. After the replacement of Ni by Pd, the shape and size of the particles changed (Fig. 2b); the SAED pattern shows the amorphous structure of the Pd/Ni–B bimetallic particles as well, in agreement with the results shown in Fig. 1a. As shown in Fig. 2c, the particle shape changed from flower-like to a solid sphere on treating the Pd/Ni–B at 200 °C, but the sample retained an amorphous structure (Fig. 1b). Compared with the Pd/Ni–B treated at 25 °C, the Pd/Ni–B treated at 200 °C had a somewhat smaller particle size and exhibited several bright dots in its corresponding SAED pattern [29], suggesting the formation of small crystalline metal clusters at 200 °C. When the treatment temperature was increased to 300 °C and then to 350 °C, more bright dots were detected in the SAED patterns (inserts in Figs. 2d and 2e), indicating that the sintering of Ni crystalline occurred. Sintering also was observed in the nano Ni and Ni–B with heating treatment, as shown in Figs. S1 (TEM images of nano Ni treated at 25, 250, and 350 °C) and S2 (TEM images of Ni–
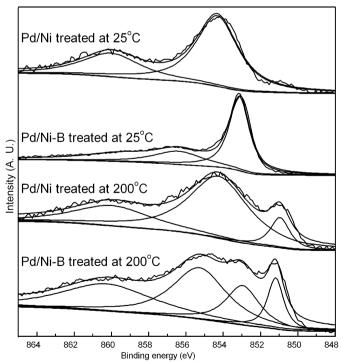

Fig. 3. XPS spectra of Ni 2p3/2 for Pd/Ni and Pd/Ni–B samples treated at different temperatures in a 40-ml/min N_2 flow.

B treated at 25 and 350 °C) in Supplementary material. These findings indicate that some polycrystalline compounds were formed at treatment temperatures above 300 °C.

Figs. 3–5 show the XPS spectra of the catalysts. The XPS intensity ratios of the metal and the support provide information on the degree of dispersion of the metal on the support [30,31].
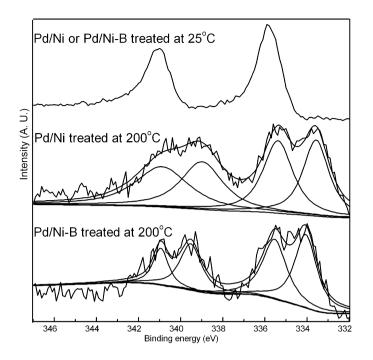
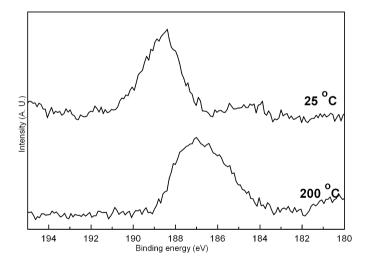**Fig. 4.** XPS spectra of Pd 3d for Pd/Ni and Pd/Ni–B treated at different temperatures in a 40-ml/min N_2 flow.

Fig. 5. XPS spectra of B 1s for Pd/Ni–B treated at different temperatures in a 40-ml/min N_2 flow.

Table 1
Surface contents of B and Pd analyzed from XPS characterization in Pd/Ni–B catalyst treated at different temperatures

Treatment temperature (°C)	Content of B (wt%)	Content of Pd (wt%)
25	6.4	4.3
200	5.2	2.1
300	5.1	1.7
350	4.9	1.0

A well-dispersed supported catalyst would show a low concentration and relative XPS intensity of active metal. Table 1 and Table S1 in Supplementary material (surface contents of Pd in Pd/Ni catalyst treated at different temperatures) present the surface concentrations of the catalysts, suggesting a decreasing surface concentration of Pd in the Pd/Ni–B and Pd/Ni particles with heating treatment. For the NiPd bulk bimetallic nanoparticles, the Pd atoms tended to aggregate on the surface of particle [32]. This decreased Pd concen-

trations resulted from two mechanisms: (i) The Pd atoms diffused into the subsurface or the bulk of Ni–B to form an alloy with increasing treatment temperature, and (ii) the Pd formed the larger Pd particles aggregated on top of the Ni–B. Wang et al. found no peaks due to crystalline Pd or Pd compounds in the XRD patterns of Pd/Ni bimetallic particles prepared via a replacement reaction and treated at 120 °C [19]. The same result also was found for the Pd/Ni bimetallic catalyst in the present study (Fig. S3 in Supplementary material), suggesting that Pd atoms were highly dispersed on the Ni surface, rather than formed into larger Pd particles [19, 20]. As shown in Fig. 1, no crystalline Pd atoms or Pd compounds were found in the Pd/Ni–B catalyst treated at different temperatures from 25 to 350 °C, indicating that the Pd atoms in Pd/Ni–B sample should be dispersed on heating treatment. On the other hand, Sra and Schaak reported the formation of AuCu and $AuCu_3$ bimetallic nanoparticle aggregates by a mixture of crystalline Au and amorphous Cu nanoparticles on aging at room temperature [15]. With increasing treatment temperature, Cu diffused into the Au bulk, forming the disordered solid solution Cu_xAu_{1-x}, and an atomically ordered AuCu was formed by heat treatment at 200 °C; thus, it was concluded that the Pd diffused into the Ni–B particles somewhat, and the Pd atoms or compounds were dispersed over the Ni–B particles.

At 850–865 eV, the Ni $2p_{3/2}$ spectra of the Pd/Ni and Pd/Ni–B samples treated at 25 °C (Fig. 3) were characterized by a main peak with a satellite at higher binding energy (BE). The main peak corresponded to the final state $2p^53d^9L^{-1}$ (L, ligand hole); the satellite peak, to a $2p^53d^8$ final state [30,31]. The BE of Ni in Pd/Ni of 854.5 eV was close to that of the Ni species in NiPd bulk bimetallic nanocluster [32]. Its satellite peak due to 860.0 eV (curve-fitted value) also was observed in the XPS spectra shown in Fig. 3. Unlike in the Pd/Ni bimetallic particles, the main peak of Ni in Pd/Ni–B was decreased to 853.2 eV, a value similar to that of amorphous Ni–B particles [33], and its satellite peak also decreased, to 856.5 eV. As shown in Fig. 3, the main and satellite Ni $2p_{3/2}$ peaks for Pd/Ni appeared at higher BEs than those for Pd/Ni–B (1.3 and 3.5 eV, respectively). However, as shown in Fig. 4, the Pd 3d spectra of Pd/Ni and Pd/Ni–B exhibited similar BEs as bulk Pd ($3d_{5/2}$, 335.8 eV and $3d_{3/2}$, 341.1 eV, [32]). These results demonstrate that the difference between Pd/Ni and Pd/Ni–B treated at 25 °C in Fig. 3 can be attributed to the alloying of Ni and B, rather than to an interaction between Pd and Ni [33]. An increased peak was observed with an increase in treatment temperature from 25 to 200 °C (Fig. 3), demonstrating the different valence state of nickel due to the alloying of Ni and Pd on heat treatment. The BE of the main peak increased from 854.5 to 854.7 eV for Pd/Ni and from 853.2 to 855.7 eV for Pd/Ni–B (curve-fitted values). This increase in BE can be attributed to the presence of Pd in the nanoparticles. For NiPd alloys, an increased BE of the main peak for Ni was observed, related to the reduced nickel d hole density due to a charge transfer from nickel to adjacent electronegative palladium [34,35]. The Pd 3d spectra of Pd/Ni and Pd/Ni–B exhibited shoulder peaks (Fig. 4). The Ni $2p_{3/2}$ spectra for the Pd/Ni and Pd/Ni–B samples showed three and four curve-fitted values, respectively (Fig. 3), and the Pd 3d spectra for Pd/Ni and Pd/Ni–B exhibited lower curve-fitted values than those treated at 25 °C (Fig. 4). These findings indicate a stronger alloying effect of Pd with Ni in the Pd/Ni–B sample, due to the structure in the amorphous nanoparticles [15,36,37] and the presence of boron [22,33]. Accurately distinguishing the valence states of the Ni species was still difficult, however.

A strong reaction and interdiffusion between the deposited Pd and the amorphous B substrate even at room temperature has been reported [38]. The BEs of the Pd $3d_{5/2}$ of the Pd/Ni–B catalyst treated at 25 °C at 335.8 and 341.1 eV (Fig. 4) were equal to those of metal Pd [32]. For the Pd/Ni catalyst treated at 200 °C, the peak
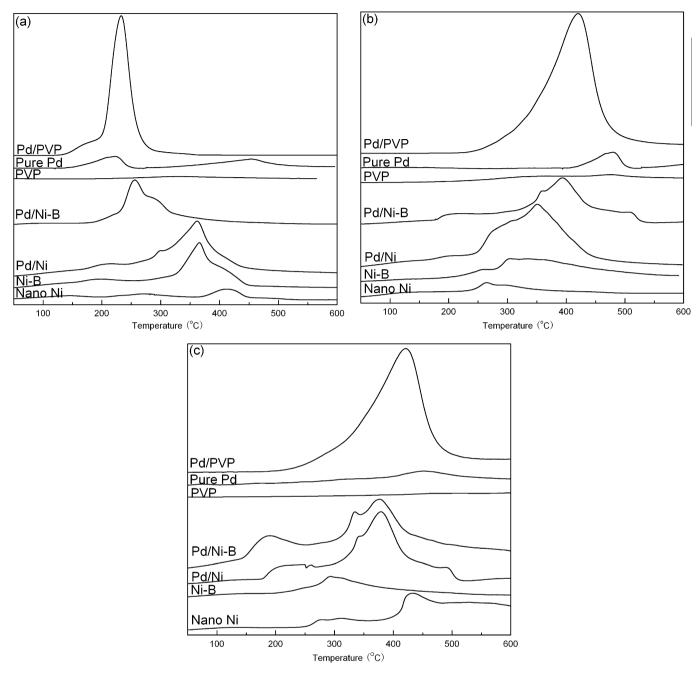
Fig. 6. TPD spectra of various catalysts. (a) Hydrogen, (b) cholorobenzene, and (c) benzene. Pure Pd was prepared by reducing PdCl$_2$ by H$_2$ gas.

of Pd 3d$_{5/2}$ was split into two peaks, one at 335.4 eV and the other at 333.5 eV; however, the peaks of Pd 3d$_{5/2}$ in the Pd/Ni–B catalyst treated at 200 °C were at 335.6 and 334.1 eV. For the Pd/Ni catalyst, the decreased BE of Pd 3d was likely due to electron donation during the transfer from Ni to Pd. In the presence of amorphous Ni–B particles, the chemical shift of the B 1s in a metal boride is influenced by B atom coordination and unoccupied d-electron states in the metal atom [38]; thus, the strong interaction between Pd and B atoms resulted in the smaller decrease in the BE of Pd to 334.1 eV, as shown in Fig. 4. This interaction has been demonstrated through an electron transfer from Pd to B atoms, resulting in the formation of palladium boride [38]. Thus, the BE of Pd in Pd/Ni–B was higher than that of Pd/Ni, as shown in Fig. 4. The B 1s spectra of the Pd/Ni–B sample are shown in Fig. 5. Fig. S4 in Supplementary material showed the XPS spectra of B 1s spectra before Ar$^+$ etching. The peak of Pd/Ni–B treated at 25 °C correspond-

ing to 188.4 eV is due to B^0 [33]. The Pd/Ni–B catalyst treated at 200 °C showed a lower peak at 187.1 eV. The decreased BE results from B's acceptance of electrons from other metal atoms. Such a shift was not observed in the treated Ni–B sample [33]. On the other hand, the reaction of crystalline Ni and B species in the solid state to produce amorphous material (known as a solid-sate amorphization reaction [SSAR]), in which B transfers electrons to Ni, has been reported [39]. Here the change in BE should be due to the interactions among Ni, Pd, and B. In short, the amorphous structure of Ni–B and the presence of B promotes the surface-alloying effect of Pd and Ni; then the surface alloy species on the Pd/Ni–B nanoparticles should be Pd–Ni–B rather than Pd–Ni.

TPD of HDC reactants and products was performed to obtain information on the relationship between HDC activity and catalyst surface properties. Fig. 6 presents the TPD spectra of H$_2$, benzene, and chlorobenzene. The H$_2$ TPD profile of the nano Ni catalyst ex-
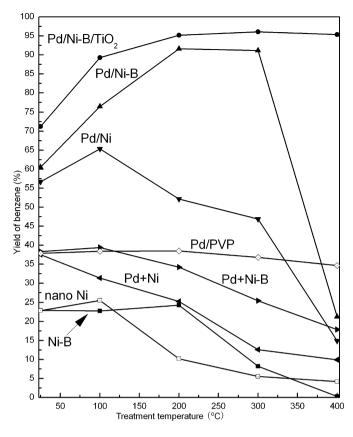
Fig. 7. Catalytic activities of catalysts treated in a 40-ml/min N_2 flow at different temperatures from 25 to 400 °C.

Table 2
HDC activities and stability of catalysts

Samples (treatment temperature)	First	Recycle 1	Recycle 2	Recycle 3	Recycle 4
Pd/Ni (25 °C)	56%	7%	–	–	–
Pd/Ni (200 °C)	53%	11%	–	–	–
Pd/Ni–B (25 °C)	60%	56%	47%	35%	6%
Pd/Ni–B (200 °C)	91%	87%	91%	71%	32%
Pd/Ni–B (300 °C)	90%	91%	88%	77%	45%
Pd/Ni–B/TiO$_2$ (200 °C)	95%	93%	94%	85%	54%

of Cl species, splitting of hydrogen molecules, and desorption of the reaction product all increased after the surface alloying of Pd with Ni. TPD of chlorobenzene and benzene for the Pd/Ni–B catalyst apparently is complex, unlike that for nano Ni. The desorption temperature of chlorobenzene increased from 300 °C (shoulder at 256 °C) over Ni–B to 395 °C (satellite 360 °C) over Pd/Ni–B. Two more peaks at 203 and 510 °C were observed in the Pd/Ni–B. The desorption temperature of benzene TPD for Ni–B was 290 °C, much lower than that of nano Ni (430 °C). This was due to the transfer of electrons from the B to the Ni atoms and the resulting enrichment of Ni with electrons, which improved the adsorption of benzene [22,23]. When Pd was deposited on the amorphous B, the Pd atoms transferred electrons to B, resulting in Pd boride [38] and a complex electron distribution over the Pd, Ni, and B. The presence of B led to the slightly higher (1–2 eV) BEs of Ni and Pd in Pd/Ni–B than in Pd/Ni. Moreover, the benzene TPD of Pd/Ni–B exhibited two main peaks at 375 (satellite 335 °C) and 175 °C, suggesting the formation of a new, more active component after Pd deposition. In our experiment, we found it difficult to distinguish these two main peaks. The desorption of hydrogen and adsorption of chlorobenzene were much greater in Pd/Ni–B than in Pd/Ni, which was ascribed to the surface alloying effect of Ni, Pd, and B, which also improved the HDC activity. The surface alloy also enhanced catalyst stability; the Pd/Ni–B catalyst could be used three times with no decrease in activity, whereas the Pd/Ni could be used only once (Table 2).

3.2. HDC activity

Fig. 7 displays the HDC activity of each catalyst studied. Nanocrystalline Ni (Fig. S1 in Supplementary material) and Ni–B demonstrated relatively low activity that decreased with increasing treatment temperature. Sintering of Ni was observed in the nano Ni and Ni–B particles treated by heating (Figs. S1 and S2 in Supplementary material). The results indicate that the HDC activity decreased with the sintering of nano Ni or Ni–B. The Pd/PVP catalyst had a ~20% higher benzene yield than the nano Ni and Ni–B catalysts. Because the particle size of Pd was stabilized by the PVP polymer, the HDC activity changed only slightly with changes in treatment temperature. The HDC activity of Pd + Ni–B (a mixture of Pd/PVP nanoparticles and Ni–B nanoparticles with weight ratio 1/99) was similar to that of Pd/PVP when both were treated at 25 °C, but decreased with increasing treatment temperature. The HDC activity of the Pd/Ni and Pd/Ni–B catalysts treated at 25 °C was similar to that of the mixtures of Pd/PVP with nano Ni or of Pd/PVP with Ni–B. The Pd/Ni–B catalyst treated at 200–300 °C demonstrated the highest HDC activity (91%), but its activity decreased with increasing treatment temperature. Table 2 displays the stability of as-prepared catalysts. Fig. 8 shows TEM images of Pd/Ni–B/TiO$_2$ prepared by the replacement reaction of Ni–B/TiO$_2$. The Pd/Ni–B in Pd/Ni–B/TiO$_2$ catalyst treated at 25 °C also exhibited a flower-like shape with a particle size of ~35 nm. The particle size changed little, but the particle shape changed to a solid sphere, with an increase in treatment temperature to 400 °C. This finding suggests that the thermal stability of Pd/Ni–B was pro-

hibited a main peak at 410 °C. Compared with nano Ni, the pure Pd showed a peak at 217 °C, indicating that the H was more weakly bonded to Pd than to Ni. The main peak of the Pd/PVP was higher (at 232 °C) than that for the pure Pd, as shown in Fig. 6a and Fig. S5 in Supplementary material. The higher temperature and larger peaks can be attributed to the different particle sizes of Pd (Fig. S6 in Supplementary material). When depositing Pd on nano Ni, the desorption peak shifted to lower temperatures 365 °C (shoulder at 300 °C), demonstrating a weaker hydrogen-bonding effect of Pd. Moreover, the area of the desorption peak increased, indicating the formation of more active sites for hydrogen splitting. As shown in Fig. 7, the HDC activity over Pd/Ni was higher than the sum of those over Pd and Ni. This suggests that the catalytic activity can be promoted by the surface alloying of Pd and Ni, in agreement with findings of Wang et al. [18–20]. Compared with the nano Ni catalyst, Ni–B had a much lower desorption temperature of H$_2$ at 360 °C (shoulder at 410 °C), due to the increased number of coordinatively unsaturated Ni sites due to the presence of B [22,23]. On replacement of Ni by Pd in the Pd/Ni–B sample, the peak corresponding to 360 °C shifted sharply to 260 °C, suggesting that the interaction of Pd with Ni–B promoted the hydrogen splitting capacity to a much greater degree than that of the Pd/Ni catalyst, due to the lower temperature of the main desorption peak for the Pd/Ni–B catalyst.

For the TPD of chlorobenzene and benzene, a desorption peak at 420 °C was observed for the Pd/PVP catalyst. The pure Pd sample exhibited a peak at 480 °C for chlorobenzene TPD and one at 450 °C for benzene TPD. The main desorption peak of chlorobenzene increased from 265 °C over nano Ni to 345 °C (shoulder at 305 °C) over Pd/Ni, with the corresponding temperatures for benzene decreasing from 275 and 430 °C to 210 and 380 °C (satellite at 340 °C). The area of peaks increased after Pd was deposited on nano Ni. These results suggest that the capacities for adsorption
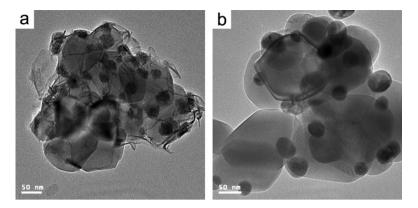
Fig. 8. TEM images of Pd/Ni–B/TiO$_2$ nanoparticles treated at a 40-ml/min N$_2$ flow. (a) Treated at 25 °C and (b) treated at 400 °C.

moted by the support. Fig. 7 and Table 2 show that the supported Pd/Ni–B/TiO$_2$ exhibited the highest HDC activity and stability.

4. Discussion

The superior catalytic activity for hydrogenation of both C=C and C=O bonds in bimetallic nanoparticles synthesized by the replacement reaction method is attributed mainly to the highly dispersed noble metal [18–20]. Generally, the HDC reaction is explained by hydrogenolysis reactions. The particle size and dispersion of active sites can affect the catalytic activity and selectivity in this reaction [10,40]. There is still no general consensus regarding the structure-sensitivity of the HDC reaction, however [40,41]. For structure-sensitive reactions, the catalytic activity and stability is thought to be related to the particle/crystal size of the active metal, rather than to the dispersion of active metal [10]. For the structure-sensitive reaction catalyzed by metal catalysts, a popular hypothesis is that the chemisorbed intermediate forms a number of bonds with the metal surface, and thus a surface site consisting of a single active metal is not adequate [42,43]. Finding a suitable array of surface atoms to accommodate such a chemisorbed intermediate poses no difficulty on a large metal crystal. On very small crystallites, however, a large fraction of the surface atoms exist at edges and corners. If the required array comprised a large number of metal atoms, then the likelihood of identifying such an array in the surface might be significantly lower than on large crystals, and the specific hydrogenolysis activity of highly dispersed metal clusters would be lower than that of large crystals [10]. This means that the reaction requires that the crystal size of the metal provide sufficient surface metal atoms to form a crystal to adsorb the intermediate. In a metal particle catalyst, crystal size is related to particle size [10], and the larger particle size of metal could provide more active sites for reactions. Some reports have suggested that the HDC of chlorobenzene over Ni catalyst is a structure-sensitive reaction [44,45]; HDC activity increases with increasing particle size, but exhibits little relation to the dispersion of Ni. As shown in Fig. 7, the HDC activity of Ni–B and Ni nanoparticles decreased with increasing treatment temperature and particle size (Figs. S1 and S2 in Supplementary material); this can be explained by the decrease in catalyst surface area. Fig. 2 shows that the Pd/Ni–B bimetallic nanoparticles grew from ∼30 to ∼50 nm with an increase in treatment temperature from 25 to 300 °C, followed by a further increase of 20–150 nm on subsequent heating to 400 °C. The HDC activity increased from 60 to 90% with an increase in the treatment temperature of Pd/Ni–B from 25 to 300 °C (Fig. 7). These findings indicate that the promotion of HDC activity is ascribed to the surface alloying effect of Pd–Ni–B, rather than to the increased particle size. Figs. 2 and 7 show a particle size of ca. 50 nm for Pd/Ni–B nanoparticles with the highest HDC activity measured.

The XPS characterization done to investigate the surface species formed in Pd/Ni–B catalyst showed that the surface alloy formed in Pd/Ni–B by heating comprised Pd, Ni, and B atoms and differed from the NiPd alloy in the Pd/Ni sample. Fig. 7 shows that the HDC activity for Pd/Ni–B was increased due to the alloying effect of Pd, Ni, and B and decreased by the NiPd alloy formed in the Pd/Ni catalyst. Moreover, Table 1 and Table S1 in Supplementary material show that the Pd surface concentrations decreased with increasing heating temperature. Thus, it can be concluded that the presence of B in the bimetallic nanoparticles mainly promoted the catalytic properties. This means that the surface alloy formed on Pd/Ni–B nanoparticles had a promoting effect on the HDC reactions. On the other hand, the HDC activity of the Pd/Ni–B catalyst increased with an increase in treatment temperature from 25 to 300 °C but decreased at treatment temperatures above 300 °C (Fig. 7). This should be related to the increased particle size, as shown in Fig. 2. Aramendía et al. found an association between the HDC of chlorobenzene and the particle size of Pd, and demonstrated that higher activity was obtained over catalysts with larger particle sizes [41]; however, in the present work, the Pd/Ni–B treated at 350 °C, which had the largest particle size, exhibited the lowest HDC activity (Fig. 2). Aramendía et al. believed that Pd's larger particle led to formation of the ρPdH phase, which should be stable under the reaction conditions [41]. The hydride phase would be an alternative source of hydrogen. These authors also noted that the larger particles should show better resistance against passivation or poisoning. The catalysts with low dispersion (i.e., those with low metal surface area and large particle size) could promote the migration of chloride species into large particles, thereby cleaning the outer surface for further reaction [40,41,44]. But we found that the hydrogen-splitting ability decreased with increasing treatment temperature, whereas the absorption ability of benzene increased (Fig. 6). This suggests that the smaller outer surface (active site) of larger particles restrains the active sites for splitting hydrogen but promotes absorption of the HDC product (benzene) (Fig. S5 in Supplementary material and Fig. 6), resulting in a low hydrogenation rate for the catalyst with larger particle size (54 ml/min hydrogenation uptake rate in Pd/Ni–B treated at 200 °C, and 30 ml/min treated at 400 °C). Here the particle size of the Pd/Ni–B with the highest HDC activity was about 50 nm, whereas that of the supported Pd/Ni–B/TiO$_2$ with the highest HDC activity was 35 nm (72 ml/min hydrogenation uptake rate), as shown in Figs. 7 and 8.

Along with its better HDC activity compared with Pd/Ni, the Pd/Ni–B catalyst also demonstrated better stability (Table 2). It was previously reported that Pd has electronegative properties in NiPd alloy [34,35]. For chlorinated aromatics, the C–Cl bond acquires a double-bond character as the chlorine atom loses p-electrons due to resonance [46]. This is followed by the formation of diadsorbed chloroaromatic species from the adsorption of chloroaromatic compounds on nickel and palladium [47,48], which are attacked by

hydride ions. For the HDC of chlorobenzene, this results in the formation of adsorbed phenyl anions, which can accept protons and thus convert to benzene [46]. The electron-deficient Pd particles are more resistant to chlorine attack as the chlorine is weakly adsorbed, due to its electrophilic character [1]. Fig. 6 shows that the deposition of Pd atoms on nano Ni increased the adsorption of chlorobenzene and splitting of hydrogen; however, the electron-enriched Pd atoms in Pd/Ni catalyst conferred considerable instability to the catalysts. This property is demonstrated by the HDC over Pd/Ni, in which the hydrogen uptake rate was as high as 67 ml/min (54 ml/min over Pd/Ni–B) initially and then rapidly decreased to about 10 ml/min (40 ml/min for Pd/Ni–B) after 10 min of reaction. This finding demonstrates that the Pd/Ni catalyst deactivated rapidly in the HDC reaction (Table 2). The Pd/Ni–B/TiO$_2$ catalyst exhibited a less-pronounced decrease in hydrogen uptake rate, from 72 to 65 ml/min after 10 min of reaction. Besides the surface alloying effect of Pd–Ni–B, the excellent activity and stability also can be attributed to the interaction between the active metal and the support [49].

5. Conclusion

In this study, bimetallic Pd/Ni–B nanoparticles were prepared by the replacement reaction. XPS and TPD characterization demonstrated the formation of a surface alloy of Pd–Ni–B. The strong surface alloying of Ni and Pd in the Pd/Ni–B catalyst was attributed to the presence of B. Compared with Pd and Pd/Ni catalysts, the Ni-Pd-B surface alloy of Pd/Ni–B exhibited increased hydrogen-splitting and chlorobenzene-adsorption capabilities, as well as increased resistance to chlorine deactivation. Thus, the Pd/Ni–B catalyst showed better activity and stability in the HDC of chlorobenzene than the Pd/Ni and Pd/PVP catalysts. An investigation of particle size in chlorobenzene HDC found an association between the HDC activity of chlorobenzene and the size of the bimetallic nanoparticles. The most suitable catalyst was the Pd/Ni–B catalyst treated at 200–300 °C, with a particle size of ∼50 nm.

Acknowledgments

Supplementary material

The online version of this article contains additional supplementary material.

Please visit DOI: 10.1016/j.jcat.2008.03.026.

References

[1] B. Coq, G. Ferrat, F. Figueras, J. Catal. 101 (1986) 434.
[2] M.L. Hitchman, R.A. Spackman, N.C. Ross, C. Agra, Chem. Soc. Rev. 95 (1995) 423.
[3] Y. Monguchi, A. Kume, K. Hattori, T. Maegawa, H. Sajiki, Tetrahedron 62 (2006) 7926.
[4] F.J. Urbano, J.M. Marinas, J. Mol. Catal. A 173 (2001) 329.
[5] R. Hara, K. Sato, W.H. Sun, T. Takahashi, Chem. Commun. 12 (1999) 845.
[6] U.R. Pillai, E.S. Sahle-Demessie, R.S. Varma, Green Chem. 6 (2004) 295.
[7] N. Lingaiah, N.S. Babu, R. Gopinath, P.S.S. Reddy, P.S.S. Prasad, Catal. Surv. Asia 10 (2006) 29.
[8] M.M. Yurii, S. Moshe, Catal. Today 75 (2002) 63.
[9] M.A. Keane, J. Chem. Technol. Biotechnol. 80 (2005) 1211.
[10] J.H. Sinfelt, Bimetallic Catalysts: Discoveries, Concepts, and Application, Wiley, New York, 1983, p. 5.
[11] M.O. Nutt, J.B. Hughes, M.S. Wong, Environ. Sci. Technol. 39 (2005) 1346.
[12] M.O. Nutt, K.N. Hechk, P. Alvarez, M.S. Wong, Appl. Catal. B 69 (2006) 115.
[13] Y.G. Sun, B.T. Mayers, Y.N. Xia, Nano Lett. 2 (2002) 481.
[14] Y.G. Sun, Z.L. Tao, J. Chen, T. Herricks, Y.N. Xia, J. Am. Chem. Soc. 126 (2004) 5940.
[15] A.K. Sra, R.E. Schaak, J. Am. Chem. Soc. 126 (2004) 6667.
[16] W.R. Lee, M.G. Kim, J.R. Choi, J.I. Park, S.J. Ko, S.J. Oh, J. Cheon, J. Am. Chem. Soc. 127 (2005) 16090.
[17] D.Y. Wang, C.H. Chen, H.C. Yen, Y.L. Lin, P.Y. Huang, B.J. Hwang, C.C. Chen, J. Am. Chem. Soc. 129 (2007) 1538.
[18] S.R. Wang, W. Lin, Y.X. Zhu, Y.C. Xie, J.G. Chen, Chin. J. Catal. 27 (2006) 301.
[19] S.R. Wang, Y.X. Zhu, Y.C. Xie, J.G. Chen, Chin. J. Catal. 28 (2007) 676.
[20] S.R. Wang, W. Lin, Y.X. Zhu, Y.C. Xie, J.R. McCormick, W. Huang, J.G. Chen, Catal. Lett. 114 (2007) 169.
[21] F. Cheng, H. Ma, Y. Li, J. Chen, Inorg. Chem. 46 (2007) 788.
[22] J.F. Deng, H.X. Li, W.J. Wang, Catal. Today 51 (1999) 113.
[23] Z.J. Wu, W. Li, M.H. Zhang, K.Y. Tao, Front. Chem. Eng. China 1 (2007) 87.
[24] X. Ni, X. Su, Z. Yang, H. Zheng, J. Cryst. Grow. 252 (2003) 612.
[25] Y. Gao, F.D. Wang, S.J. Liao, D.R. Yu, N. Sun, React. Funct. Polym. 44 (2000) 65.
[26] Z.Y. Li, C.H. Han, J.Y. Shen, J. Mater. Sci. 41 (2006) 3473.
[27] Z.J. Wu, M.H. Zhang, S.H. Ge, Z.L. Zhang, W. Li, K.Y. Tao, J. Mater. Chem. 15 (2005) 4928.
[28] Z.J. Wu, S.H. Ge, M.H. Zhang, W. Li, S.C. Mu, K.Y. Tao, J. Phys. Chem. C 111 (2007) 8587.
[29] N. Hedgecock, P. Tung, M. Schlesinger, J. Electrochem. Soc. 122 (1975) 866.
[30] J.P. Espinos, J. Morales, A. Barranco, A. Caballero, J.P. Holgado, A.R. Gonzalez-Elipe, J. Phys. Chem. B 106 (2002) 6921.
[31] A.R. Naghash, T.H. Etsell, S. Xu, Chem. Mater. 18 (2006) 2480.
[32] P. Lu, T. Teranishi, K. Asakura, M. Miyake, N. Toshima, J. Phys. Chem. B 103 (1999) 9673.
[33] H. Li, H.X. Li, W.L. Dai, W.J. Wang, Z.G. Fang, J.F. Deng, Appl. Surf. Sci. 152 (1999) 25.
[34] G. Treglia, M.C. Desjonqueres, F. Duncastelle, D. Spanjaand, J. Phys. C 14 (1981) 4347.
[35] K. Kishi, Y. Motoyoshi, S. Ikeda, Surf. Sci. 105 (1982) 313.
[36] R.E. Schaak, A.K. Sra, B.M. Leonard, R.E. Cable, J.C. Bauer, Y.F. Han, J. Means, W. Teizer, Y. Vasquez, E.S. Funck, J. Am. Chem. Soc. 127 (2005) 3506.
[37] R.E. Cable, R.E. Schaak, J. Am. Chem. Soc. 128 (2006) 9588.
[38] D.H. Shen, P.A. Kearney, J.M. Slaughter, C.M. Falco, J. Magn. Magn. Mater. 126 (1993) 25.
[39] A.N. Campbell, J.C. Barbour, C.R. Hills, J. Mater. Res. 4 (1989) 1303.
[40] F.H. Ribeiro, C.A. Gerken, G. Rupprechter, G.A. Somorjai, C.S. Kellner, G.W. Coulston, L.E. Manzer, L. Abrams, J. Catal. 176 (1998) 352.
[41] M.A. Aramendía, V. Boráu, I.M. García, C. Jiménez, F. Lafont, A. Marinas, J.M. Marinas, F.J. Urbano, J. Catal. 187 (1999) 392.
[42] J.H. Sinfelt, J.L. Carter, D.J.C. Yates, J. Catal. 24 (1972) 283.
[43] V. Ponec, W.M.H. Sachtler, J. Catal. 24 (1972) 250.
[44] Y.H. Choi, W.Y. Lee, Catal. Lett. 67 (2000) 155.
[45] M.A. Keane, C. Park, C. Menini, Catal. Lett. 88 (2003) 89.
[46] V.A. Yakovlev, V.V. Terskikh, V.I. Simagina, V.A. Likholobov, J. Mol. Catal. A 153 (2000) 231.
[47] R.B. LaPierre, D. Wu, W.L. Kranich, J. Catal. 52 (1978) 59.
[48] R.B. LaPierre, L. Guczi, W.L. Kranich, J. Catal. 52 (1978) 230.
[49] S.J. Tauster, S.C. Fung, R.L. Garten, J. Am. Chem. Soc. 100 (1978) 170.